Tunneling Barrier Thickness Dependence of Spin Polarization of Ferromagnet in Magnetic Tunnel Junctions

Yu-Qing Zhao(赵宇清)[1], Hai-Yan Zuo(左海艳)[1], Shao-Wei Li(李少薇)[1], Ke Xia(夏珂)[2], Ming Wen(闻明)[3], Jun-Mei Guo(郭俊梅)[3], Peng Xiong[4], and Cong Ren(任聪)[1,5*]

[1]*School of Physics and Astronomy, Yunnan University, Kunming 650500, China*
[2]*Department of Physics, Southeast University, Nanjing 100193, China*
[3]*Kunming Institute of Precious Metals, Kunming 650019, China*
[4]*Physics Department, Florida State University, Tallahassee, USA*
[5]*Yunnan Key Laboratory of Eletromagnetic Materials and Devices, Yunnan University, Kunming 650500, China*

(Received 26 July 2024; accepted manuscript online 30 September 2024)

For designing low-impedance magnetic tunnel junctions (MTJs), it has been found that tunneling magnetoresistance strongly correlates with the insulating barrier thickness, imposing a fundamental problem about the relationship between spin polarization of ferromagnet and the insulating barrier thickness in MTJs. Here, we investigate the influence of alumina barrier thickness on tunneling spin polarization (TSP) through a combination of theoretical calculations and experimental verification. Our simulating results reveal a significant impact of barrier thickness on TSP, exhibiting an oscillating decay of TSP with the barrier layer thinning. Experimental verification is realized on FeNi/AlO_x/Al superconducting tunnel junctions to directly probe the spin polarization of FeNi ferromagnet using Zeeman-split tunneling spectroscopy technique. These findings provide valuable insights for designs of high-performance spintronic devices, particularly in applications such as magnetic random access memories, where precise control over the insulating barrier layer is crucial.

DOI: 10.1088/0256-307X/41/11/117201

Magnetic tunnel junctions (MTJs) are characterized by an insulating tunnel barrier layer situated between ferromagnetic electrodes. The primary mechanism behind the observed tunneling magnetoresistance (TMR) is coherent tunneling,[1–3] which modifies resistance through the alignment of electron spins (parallel or antiparallel). This process underscores the crucial interplay between spin dynamics and charge transport, essential for advancing spintronic devices. Achieving a significant TMR ratio is paramount for the efficacy of high-performance devices, particularly in applications such as magnetic random access memories (MRAMs) and highly sensitive magnetic field sensors.[4–9] Additionally, the development of non-volatile and high-density MRAMs necessitates minimizing the volume of magnetic tunnel junctions. A pivotal strategy involves controlling both the barrier thickness to reduce the junction impedance and the thickness of magnetic thin films to induce perpendicular magnetic anisotropy (PMA),[10–13] crucial at the nanoscale for mitigating demagnetizing effects and enhancing thermal stability. This adjustment reduces the critical current required in voltage-controlled MRAMs and lowers the write error rate.

Moreover, extensive research on traditional MTJ magnetic layers is aimed at enhancing the TMR ratio and expanding their application scope. This includes optimizing insulating barrier materials to achieve low resistance (about $1\,\Omega\cdot\mu m^2$) and a significant TMR ratio (over 100%) at room temperature.[14] For a target recording density of $1\,Tbit/in^2$, a magnetoresistance (MR) ratio above 70% at a junction resistance RA (R-resistance, A-junction area) product of approximately $0.6\,\Omega\cdot\mu m^2$ is required. In the field of spintronics, the coherent tunneling properties of MgO, coupled with the half-metallicity of body-centered cubic (bcc) ferromagnetic electrodes such as Fe and/or CoFeB, have made CoFeB/MgO/CoFeB the preferred configuration for MTJs.[15] Extensive studies on these junctions have demonstrated that junction resistance RA and TMR are inversely related; as RA decreases, so does TMR.[16–19] Additionally, reducing the MgO layer thickness by 0.5 nm can decrease the junction resistance by an order of magnitude, underscoring the importance of precise control over barrier thickness for optimal junction performance.

In this study, we utilized the $Ni_{1-x}Fe_x$ alloy as the ferromagnetic electrode. By integrating theoretical calculations with experimental methods, we explored the impact of the metal oxide barrier layer thickness on tunneling spin polarization (TSP). TMR and TSP are closely related and effectively described by the Julliere formula: $\mathrm{TMR} = \frac{2P_1P_2}{1-P_1P_2}$,[20] where $P_{1(2)} = \frac{G_{\uparrow 1(2)}-G_{\downarrow 1(2)}}{G_{\uparrow 1(2)}+G_{\downarrow 1(2)}}$ denotes the spin polarization of the respective ferromagnetic electrodes. Our research aims to thoroughly understand the relationship between TSP and barrier thickness, to explain TMR variation with RA changes and achieve a balance between high recording density and thermal stability. Our findings reveal that a decrease in barrier layer thickness

*Corresponding author. Email: cren@ynu.edu.cn
© 2024 Chinese Physical Society and IOP Publishing Ltd

leads to a reduction in TSP. Combining this observation with the Julliere formula indicates that TMR is influenced by changes in the barrier layer thickness due to the variations in TSP. Consequently, identifying an optimal barrier layer thickness is essential to ensure high TMR while managing junction resistance, as evidenced by our experimental verification by superconducting tunnel junctions.

Unlike typical chaotic modeling processes, our approach is structured and orderly influenced by the methodology outlined in Refs. [21–23]. We constructed a superlattice structure by integrating the α-Al_2O_3 (0001) ($R3c$ space group) with the (111) plane of $FeNi_3$ and Cu ($Pm3m$ space group). This structural assembly leads to the formation of the $FeNi_3/\alpha$-Al_2O_3/Cu junction, consisting of 6 layers (each containing magnetic metal $FeNi_3$ and Cu), in addition to a variable number of α-Al_2O_3 (0001) facet layers, creating a sophisticated double-probe tunnel junction. The in-plane lattice constant is meticulously maintained at 0.5002 nm, with a lattice mismatch rate close to 5%. The Ni–O and Cu–O distances are precisely set at 0.168 nm and 0.167 nm, respectively.

As shown in Fig. 1, $FeNi_3/\alpha$-Al_2O_3/Cu junction investigated in this work is two-probe tunnel junction, consisting of magnetic metal $FeNi_3$, normal metal Cu and several monolayer of α-Al_2O_3 barriers. We fix the positions of the outermost three layers and conduct optimization using a $9 \times 9 \times 1$ k-point grid. The optimal model of the $FeNi_3/\alpha$-Al_2O_3/Cu junction, including its electronic and magnetic characteristics, was determined through density functional theory (DFT) calculations within the Quantum Espresso.[24–26] These calculations utilize the Perdew–Burke–Ernzerhof[27] variant of the generalized gradient approximation for solving the exchange-correlation function. We adopt a plane wave energy cutoff of 60 Ry for precise accuracy.

Our analysis extends to quantum transport calculations via the non-equilibrium Green's Function-density functional theory (NEGF-DFT) method. This approach integrates real-space DFT with the Keldysh NEGF formalism, as implemented in the Nanodcal package.[28] Throughout the transport calculation phase, the atomic basis functions are represented by a linear combination of atomic orbital (LCAO) methodology, with a double zeta plus polarization (DZP) orbital basis set. We address the exchange-correlation energy through the local density approximation (LDA), incorporating linear spin polarization and selecting a cutoff energy of 60 Ry. Through these calculations, we derive wave-vector resolved conductances for electrodes in spin-up and spin-down magnetization states, denoted as $G_\uparrow(k_\parallel)$ and $G_\downarrow(k_\parallel)$, where $\uparrow$ ($\downarrow$) signifies the up-spin (down-spin) channel. Herein, the up-spin (down-spin) channel corresponds to the majority (minority) spin channel of the left electrode. The average conductance, exemplified as $G_\uparrow = \sum_{k_\parallel} G_\uparrow(k_\parallel)/N$, where N represents the count of $k_\parallel$ points sampled, is calculated. Upon ensuring satisfactory convergence of both channel conductance, with N established at 300×300, we proceed to calculate the tunneling spin polarization (TSP).

Using the Nanodcal software, we have explored the relationship between conductivity and the thickness of the barrier layer for the majority ($G_\uparrow(k_\parallel)$) and minority ($G_\downarrow(k_\parallel)$) spin channels in MTJs under zero-bias conditions. Employing the equation $P_{1(2)} = \frac{G_{\uparrow 1(2)} - G_{\downarrow 1(2)}}{G_{\uparrow 1(2)} + G_{\downarrow 1(2)}}$, we derive TSP with varying barrier layer thickness. Our comprehensive analysis is detailed in Table 1.

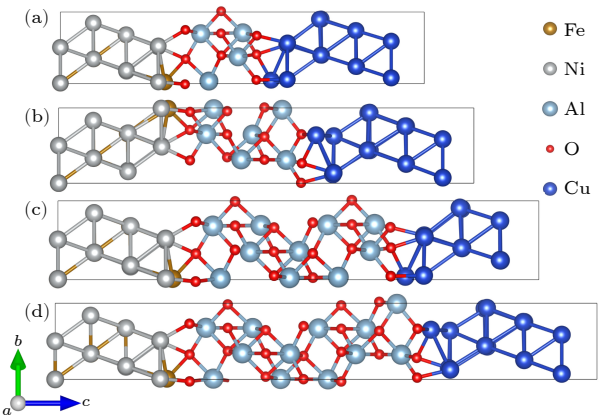

Fig. 1. Four optimized junction structure with different alumina thicknesses of a $FeNi_3/\alpha$-Al_2O_3/Cu(111) tunnel junction model. The transport direction is along the c-axis while the tunnel junction is periodic along the a- and b-directions. The thicknesses of the alumina are 0.437, 0.644, 1.312 nm. The optimized $FeNi_3$-O distance and the thickness of the Al_2O_3 (in units of nm) are marked.

Table 1. Calculated conductances and TSP. The units are in e^2/h and %, respectively.

d (nm)	Minor spin	Major spin	TSP
0.437	2.87×10^{-2}	4.21×10^{-2}	18.92
0.571	4.5×10^{-3}	9.9×10^{-3}	37.5
0.644	1.9×10^{-3}	6.4×10^{-3}	54.21
0.741	3.7412×10^{-4}	1.2×10^{-3}	52.46
0.874	3.2163×10^{-4}	9.5977×10^{-4}	49.80
1.093	3.3892×10^{-5}	1.3379×10^{-4}	59.57
1.312	5.2007×10^{-6}	1.7563×10^{-5}	53.60
1.530	5.6403×10^{-7}	1.9698×10^{-6}	55.48

As depicted in Figs. 2(a)–2(d), the conductance of $FeNi_3$ (111)/α-Al_2O_3/Cu_3 tunnel junctions, along with the plane wave vector (k_x, k_y), is explored under two barrier thicknesses 0.571 and 1.093 nm. Figures 2(a) and 2(c) specifically illustrate the conductance distribution of the majority spin channels across the $k_x a/2\pi$ and $k_y a/2\pi$ planes for barrier thicknesses respectively. In both scenarios, conductance is concentrated around the central region, with $(k_x, k_y) = (0, 0)$. In Figs. 2(b) and 2(d) for the minority spin channels, $G_\downarrow(k_\parallel)$ shows negligible values at (0, 0) and a broader distribution across the Brillouin zone compared to those of $G_\uparrow(k_\parallel)$.

Figure 2(e) summarizes the calculated TSP as a function of α-Al_2O_3 layer thickness d. As is shown, a significant reduction in TSP occurs falling sharply from 54% to 18% as the barrier thickness decreases from 0.74 nm to 0.43 nm. Within this range, $G_\downarrow(k_\parallel)$ decays more rapidly than $G_\uparrow(k_\parallel)$, indicating high sensitivity of minority spins to barrier changes. Conversely, when the barrier thickness

exceeds 0.8 nm, the decay rates of conductances for both spin channels start to align, causing TSP values to rapidly saturate as the barrier thickens. This uniformity at larger thicknesses indicates a more stable impact of the barrier on spin-dependent tunneling, maintaining consistent TSP values.

To quantitatively describe the decaying behavior of the calculated TSP with Al_2O_3-barrier thickness, a phenomenological formula is proposed as follows:[29]

$$P = P_0 + \alpha e^{-\beta d}, \tag{1}$$

where P_0 represents the saturated value, and β^{-1} denotes the overall TSP decaying length. Based on Eq. (1), we determine that the calculated TSP gradually approaches $P_0 = 54.8 \pm 0.05\%$, and identify critical parameters, including $\alpha = -0.5 \pm 0.05$ and $\beta = 0.8219\,\mathrm{nm}^{-1}$.

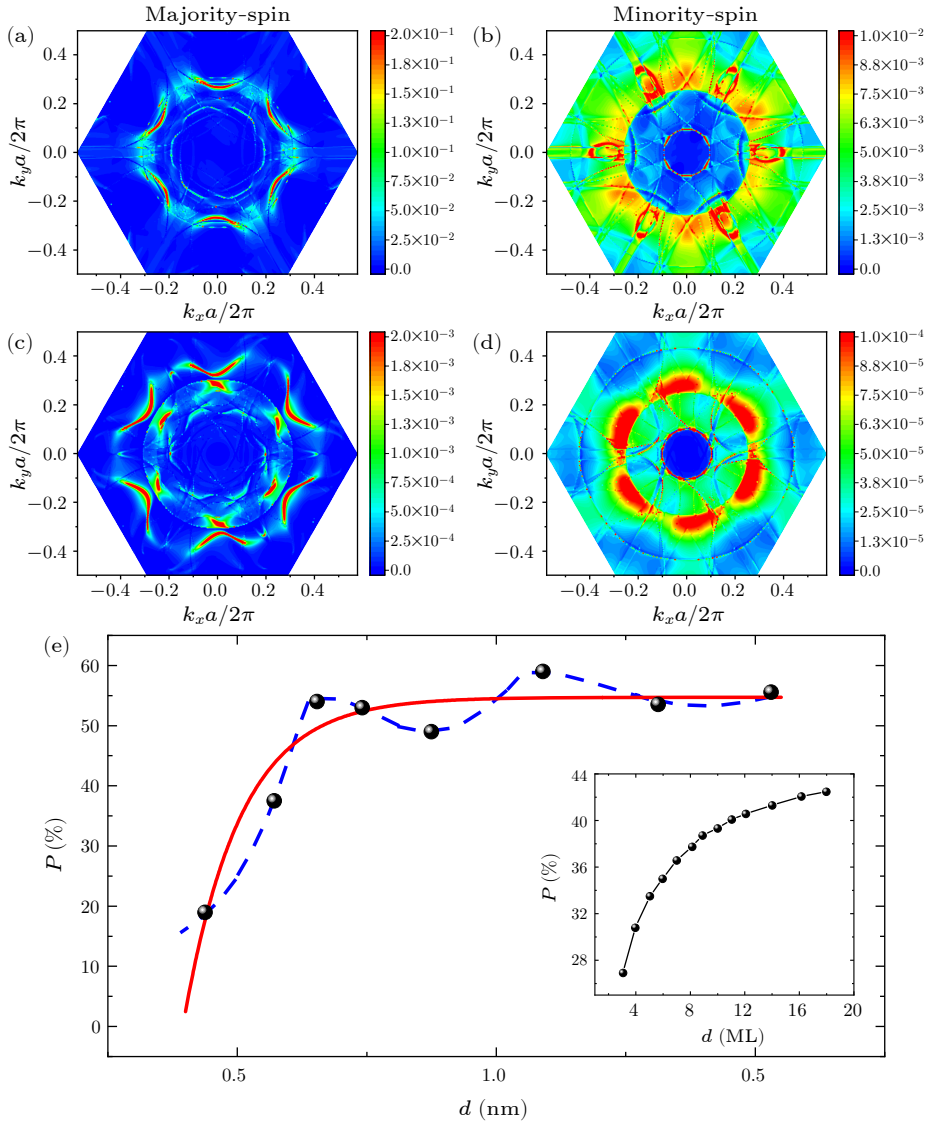

Fig. 2. Dependence of conductance on $k_\parallel$ in $FeNi_3$(111)/vacuum/Cu(111) tunnel junctions. [(a), (b)] Majority-spin conductance $G_\uparrow(k_\parallel)$ and minority-spin conductance $G_\downarrow(k_\parallel)$ for an Al_2O_3 thickness of 0.571 nm. [(c), (d)] Spin conductance $G_\uparrow(k_\parallel)$ and $G_\downarrow(k_\parallel)$ for an Al_2O_3 thickness of 1.093 nm. (e) Total tunneling spin polarization as a function of barrier thickness d for the $FeNi_3$(111)/Al_2O_3/Cu(111) tunnel junction. The red solid line is the least-square fitting of the calculated TSP data. The blue dashed line is a guide to the eyes. Inset: the calculated TSP as a function of the thickness of vacuum barrier for a $FeNi_3$(111)/vacuum/Cu(111) tunnel junction.

A remarkable feature is that oscillating behavior in the calculated TSP superimposes on its decaying curve with the thickness of Al_2O_3-barrier layer, as shown in Fig. 2(e). The oscillatory period TSP may reflect the decaying length of α-Al_2O_3. This could be attributed to coherent tunneling in crystalline-layered Al_2O_3 barrier, which likely minimizes electron scattering from interfacial defects and lattice mismatch. To strengthen our conclusions, we perform a similar calculation on $FeNi_3$(111)/-Cu(111) tunnel junctions in vacuum as the insulating barrier, to completely neglect interfacial matching effect. In the inset of Fig. 2(e), we present the electronic structure analysis of the $FeNi_3$(111)/vacuum/Cu(111) junction using the tight-binding (TB) model coupled with the coher-

ent potential approximation. As is shown, the oscillatory TSP disappears, remaining of a decaying TSP, as the vacuum barrier layer thickness is reduced from 20 monolayers (ML) to 5 ML (1 ML $\simeq$ 0.2 nm). This attenuation pattern aligns qualitatively with our findings in Al_2O_3-barrier tunnel junction, suggesting that the spin polarization of MTJ components is not inherently stable but increases with the barrier thickness until reaching a saturation point.

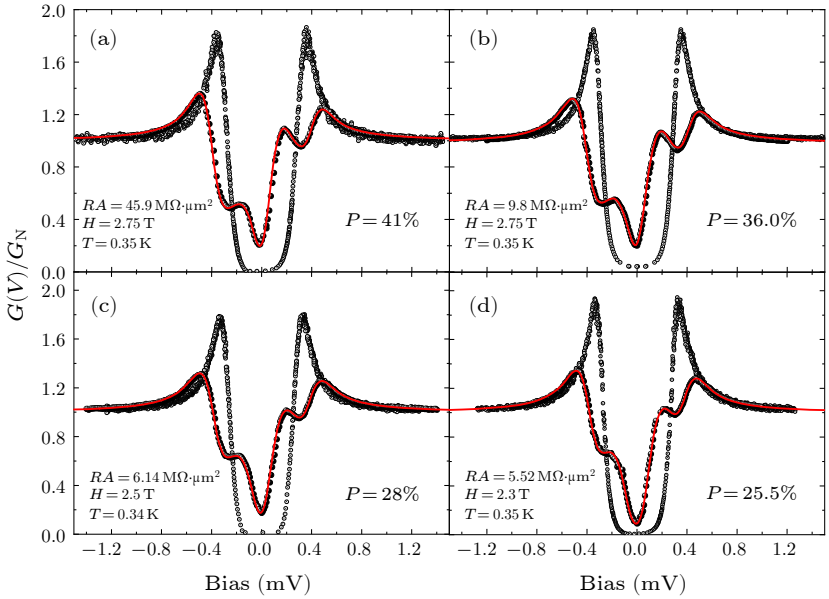

Fig. 3. (a) Tunneling conductance dI/dV versus bias voltage V for junctions with different RA at base temperature $T = 0.34$ K in zero field (filled symbols) and magnetic fields (open symbols). The solid curves are the fits to the data measured in magnetic fields using Maki's theory as described in the text.

To experimentally verify our calculation results that TSP of ferromagnetic electrode in MTJs decays with the thinned barrier layer, we prepared a series of $Fe_{20}Ni_{80}/AlO_x/Al$ tunnel junctions to directly probe the spin polarization of $Fe_{20}Ni_{80}$ as a function of the thickness of AlO_x-barrier layer. Planar tunnel junctions made of $Al/AlO_x/Fe_{20}Ni_{80}$ with the size of 200 μm wide and 4 nm thick Al were thermally evaporated on pieces of Corning glass substrate. A series of AlO_x-barrier was formed by naturally oxidizing Al in pure oxygen gas in 120 h to 30 min. Then a 50-nm-thick $Fe_{20}Ni_{80}$ layer was magnetically sputtered with 200 μm in width on top of the Al/AlO_x layer. Samples were further post-annealed at 160°C for 5 min in a high vacuum chamber to repair pinholes in the insulating layer. It is noted that the insulating AlO_x barrier formed in this way is amorphous with varying thickness.

Figure 3 shows the main results of our experiment, i.e., tunneling conductance $G(V) \equiv dI/dV$ versus bias voltage V for junctions with different junction resistance at $T = 0.34$ K in zero and finite magnetic fields. For all junctions, the tunneling conductance curves at zero field clearly reveal the superconducting energy gap Δ of the superconducting Al. In the presence of a parallel magnetic field, the superconducting density of states (DOS) of Al is Zeeman-split, and can be expressed as [30,31]

$$\rho_{\uparrow\downarrow} = \frac{\rho(0)}{2}\mathrm{Im}\Big(\frac{u_\pm}{\sqrt{1-u_\pm}}\Big), \tag{2}$$

with $\rho(0)$ being the normal-state DOS of the superconductor at E_F. Here, $u_\pm$ are found by solving the following set of coupled complex equations: [32]

$$u_\pm = \frac{E \mp \mu_B H}{\Delta} + \frac{\zeta u_\pm}{\sqrt{1-u_\pm^2}} + b\left(\frac{u_\mp - u_\pm}{\sqrt{1-u_\mp^2}}\right). \tag{3}$$

Here, E is the energy with respect to E_F, Δ is the superconducting energy gap, ζ is the orbital depairing parameter, b the spin-orbit parameter, [30,31] and μ_B is the magnetic moment of the electron. Under such a scheme of probing interfacial spin polarization, the normalized conductance curves is generalized as follows: [32]

$$\frac{G(V)}{G_N} = \frac{1}{8k_BT}\int_{-\infty}^{+\infty}\Big[\Big(\frac{1+P}{2}\Big)\rho_\uparrow + \Big(\frac{1-P}{2}\Big)\rho_\downarrow\Big] \times \mathrm{sech}^2\Big(\frac{E+eV}{k_BT}\Big)dE. \tag{4}$$

Excellent fits are obtained for all junctions with appropriate values for b and ζ. For high resistance junctions, the extracted P is around 41%. With decreasing junction resistance RA, P drops systematically, reaching a value of 25.5% with $RA = 5.52\,\mathrm{M\Omega}\cdot\mu\mathrm{m}^2$. To obtain the barrier thickness, RA can be obtained by using the Simmons or Brinkman Dynes-Rowell formula, in the limit where bias voltage $V \to 0$: [33,34] $RA = 3.17 \times (d/\phi^{1/2})\exp(1.025d\phi^{1/2})$. Here RA is in units of $\mathrm{M\Omega}\cdot\mu\mathrm{m}^2$, ϕ is in eV and d in nm. To compare directly with the MTJs, we used a barrier height of 1.8 eV for our AlO_x barriers. [35,36] Consequently, the barrier thickness is determined to be 1.75 nm for the junction with $RA = 45.9\,\mathrm{M\Omega}\cdot\mu\mathrm{m}^2$.

The values of TSP are plotted as a function of the barrier thickness in Fig. 4. It is obvious that TSP begins to decrease drastically below the AlO_x barrier thickness of 1.1 nm. By fitting to Eq. (1), it is obtained that $P_0 = 41\%$, $\alpha = -10.74$ and $\beta = 0.5336\,\mathrm{nm}^{-1}$. This leads to a decaying length of 1.87 nm for overall TSP of the $Fe_{20}Ni_{80}$-amorphous AlO_x system.

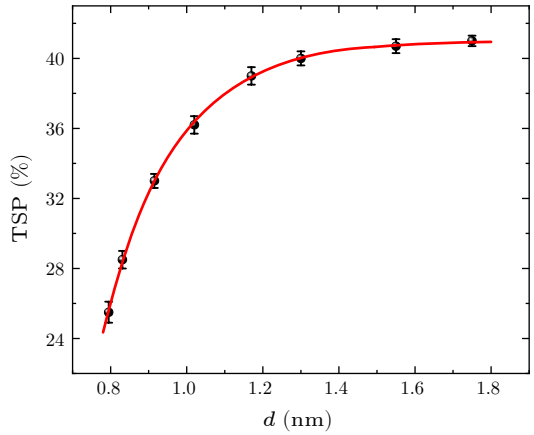

Fig. 4. Extracted spin polarization P versus the barrier thickness. The error bars for P are from the averaged value to fit to the curves in Fig. 3, and for d from the averaged barrier thickness of using 1.8 eV for barrier height. The solid line is the fit to the data using Eq. (1).

In conclusion, we extensively examined the impact of insulating barrier thickness on TSP of ferromagnet in MTJs through a combination of theoretical calculations and experimental verification. Our findings revealed that the alumina barrier thickness significantly influences TSP, showing periodic oscillations with changes in the number of atomic layers. We observed an oscillatory decay behavior of the spin polarization rate as the barrier thickness varied, closely related to the crystal structure of α-Al_2O_3 and the $FeNi_3/Al_2O_3$ interface.

Through experimental validation using Zeeman-split tunneling spectroscopy on $FeNi/AlO_x/Al$ systems, we confirmed our theoretical predictions, demonstrating that the polarization systematically decreases with the thinning of the tunnel barrier. This reduction in spin polarization is attributed to the effective tunneling of negative spin polarization currents generated by d-like interface states. According to a simple and approximate relationship between the spin polarization and the tunnel barrier thickness measured experimentally, it can be used to validate the calculation results of the two different models of $FeNi_3/\alpha$-Al_2O_3/Cu and $FeNi_3$/vacuum/Cu. The difference between the TSP calculated at Py/Al_2O_3 and Py/vacuum shows that TSP is determined not only by ferromagnetic materials but also by the thickness of the barrier layer and the FM/I interface.

These insights are crucial for the design and development of low-impedance MTJs, particularly for applications in MRAMs, where precise control over the insulating barrier layer is essential for achieving high TMR ratio and low junction resistance.

Acknowledgements. The authors thank P. Schlottmann for his contributions in the analysis of the Zeeman-split tunneling spectroscopy. This work was supported by the National Natural Science Foundation of China (Grant Nos. 11774303 and 11574373). Yu-qing Zhao thanks the financial support from "15th Graduate Research Innovation Project" from Yunnan University. C.R. acknowledges financial support from the Joint Fund of Yunnan Provincial Science and Technology Department (Grant No. 2019FY003008).

References

[1] Moodera J S, Kinder L R, Wong T M, and Meservey R 1995 *Phys. Rev. Lett* **74** 3273
[2] Butler W H, Zhang X G, Schulthess T C, and MacLaren J M 2001 *Phys. Rev. B* **63** 054416
[3] Mathon J and Umerski A 2001 *Phys. Rev. B* **63** 220403(R)
[4] Dieny B and Chshiev M 2017 *Rev. Mod. Phys.* **89** 025008
[5] Hellman F *et al.* 2017 *Rev. Mod. Phys.* **89** 025006
[6] Brataas A, Kent A D, and Ohno H 2012 *Nat. Mater.* **11** 372
[7] Kent A D and Worledge D C 2015 *Nat. Nanotechnol.* **10** 187
[8] Wang M X, Cai W L, Zhu D Q, Wang Z H, Kan J, Zhao Z Y, Cao K H, Wang Z L, Zhang Y G, Zhang T R, Park C, Wang J P, Fert A, and Zhao W S 2018 *Nat. Electron.* **1** 582
[9] Borders W A, Pervaiz A Z, Fukami S, Camsari K Y, Ohno H, and Datta S 2019 *Nature* **573** 390
[10] Apalkov D, Dieny B, and Slaughter J M 2016 *Proc. IEEE* **104** 1796
[11] Worledge D C, Hu G, Abraham D W, Sun J Z, Trouilloud P L, Nowak J, Brown S, Gaidis M C, O'Sullivan E J, and Robertazzi R P 2011 *Appl. Phys. Lett.* **98** 022501
[12] Ikeda S, Miura K, Yamamoto H, Mizunuma K, Gan H D, Endo M, Kanai S, Hayakawa J, Matsukura F, and Ohno H 2010 *Nat. Mater.* **9** 721
[13] Masuda K, Itoh H, Sonobe Y, Sukegawa H, Mitani S, and Miura Y 2021 *Phys. Rev. B* **103** 064427
[14] Nagamine Y, Maehara H, Tsunekawa K, Djayaprawira D D, Watanabe N, Yuasa S, and Ando K 2006 *Appl. Phys. Lett.* **89** 162507
[15] Parkin S S P, Kaiser C, Panchula A, Rice P M, Hughes B, Samant M, and Yang S H 2004 *Nat. Mater.* **3** 862
[16] Yuasa S, Nagahama T, Fukushima A, Suzuki Y, and Ando K 2004 *Nat. Mater.* **3** 868
[17] Tsunekawa K, Djayaprawira D D, Nagai M, Maehara H, Yamagata S, Watanabe N, Yuasa S, Suzuki Y, and Ando K 2005 *Appl. Phys. Lett.* **87** 072503
[18] Maehara H, Nishimura K, Nagamine Y, Tsunekawa K, Seki T, Kubota H, Fukushima A, Yakushiji K, Ando K, and Yuasa S 2011 *Appl. Phys. Express* **4** 033002
[19] Scheike T, Xiang Q Y, Wen Z C, Sukegawa H, Ohkubo T, Hono K, and Mitani S 2021 *Appl. Phys. Lett.* **118** 042411
[20] Julliere M 1975 *Phys. Lett. A* **54** 225
[21] Jennison D R, Verdozzi C, Schultz P A, and Sears M P 1999 *Phys. Rev. B* **59** R15605
[22] Jung H, Kim Y, Jung K, Im H, Pashkin Y A, Astafiev O, Nakamura Y, Lee H, Miyamoto Y, and Tsai J S 2009 *Phys. Rev. B* **80** 125413
[23] Diesková M Z, Ferretti A, and Bokes P 2013 *Phys. Rev. B* **87** 195107
[24] Giannozzi P, Andreussi O, Brumme T, Bunau O, Buongiorno Nardelli M, Calandra M, Car R, Cavazzoni C, Ceresoli D, Cococcioni M, Colonna N, Carnimeo I, Dal Corso A, de Gironcoli S, Delugas P, DiStasio R A, Ferretti A, Floris A, Fratesi G, Fugallo G, Gebauer R, Gerstmann U, Giustino F, Gorni T, Jia J, Kawamura M, Ko H Y,

Kokalj A, Küçükbenli E, Lazzeri M, Marsili M, Marzari N, Mauri F, Nguyen N L, Nguyen H V, Otero-de-la-Roza A, Paulatto L, Poncé S, Rocca D, Sabatini R, Santra B, Schlipf M, Seitsonen A P, Smogunov A, Timrov I, Thonhauser T, Umari P, Vast N, Wu X and Baroni S 2017 *J. Phys.: Condens. Matter* **29** 465901

[25] Giannozzi P, Baroni S, Bonini N, Calandra M, Car R, Cavazzoni C, Ceresoli D, Chiarotti G L, Cococcioni M, Dabo I, Dal Corso A, de Gironcoli S, Fabris S, Fratesi G, Gebauer R, Gerstmann U, Gougoussis C, Kokalj A, Lazzeri M, Martin-Samos L, Marzari N, Mauri F, Mazzarello R, Paolini S, Pasquarello A, Paulatto L, Sbraccia C, Scandolo S, Sclauzero G, Seitsonen A P, Smogunov A, Umari P and Wentzcovitch R M 2009 *J. Phys.: Condens. Matter* **21** 395502

[26] Giannozzi P, Baseggio O, Bonfà P, Brunato D, Car R, Carnimeo I, Cavazzoni C, de Gironcoli S, Delugas P, Ruffino F F, Ferretti A, Marzari N, Timrov I, Urru A, and Baroni S 2020 *J. Chem. Phys.* **152** 154105

[27] Perdew J P, Burke K, and Ernzerhof M 1996 *Phys. Rev. Lett.* **77** 3865

[28] Taylor J, Guo H, and Wang J 2001 *Phys. Rev. B* **63** 245407

[29] Münzenberg M and Moodera J S 2001 *Phys. Rev. B* **70** 060402(R)

[30] Maki K and Fulde P 1965 *Phys. Rev.* **140** A1586

[31] Monsma D J and Parkin S S P 2000 *Appl. Phys. Lett.* **77** 883

[32] Worledge D C and Geballe T H 2000 *Phys. Rev. B* **62** 447

[33] Esaki L 1969 *Tunneling in Solids.* In: Haidemenakis E D (eds) *Electronic Structures in Solids* (Boston, MA: Springer) p 135

[34] Brinkman W F, Dynes R C, and Rowell J M 1970 *J. Appl. Phys.* **41** 1915

[35] Åkerman J J, Slaughter J M, Dave R W, and Schuller I K 2001 *Appl. Phys. Lett.* **79** 3104

[36] Liu X Y, Ren C, Ritchie L, Schrag B D, Xiao G, and Li L F 2003 *J. Magn. Magn. Mater.* **267** 133